A New Two-Moment Bulk Stratiform Cloud Microphysics Scheme in the Community Atmosphere Model, Version 3 (CAM3). Part I: Description and Numerical Tests

HUGH MORRISON AND ANDREW GETTELMAN

National Center for Atmospheric Research, Boulder, Colorado*

(Manuscript received 18 June 2007, in final form 4 January 2008)

ABSTRACT

A new two-moment stratiform cloud microphysics scheme in a general circulation model is described. Prognostic variables include cloud droplet and cloud ice mass mixing ratios and number concentrations. The scheme treats several microphysical processes, including hydrometeor collection, condensation/evaporation, freezing, melting, and sedimentation. The activation of droplets on aerosol is physically based and coupled to a subgrid vertical velocity. Unique aspects of the scheme, relative to existing two-moment schemes developed for general circulation models, are the diagnostic treatment of rain and snow number concentration and mixing ratio and the explicit treatment of subgrid cloud water variability for calculation of the microphysical process rates.

Numerical aspects of the scheme are described in detail using idealized one-dimensional offline tests of the microphysics. Sensitivity of the scheme to time step, vertical resolution, and numerical method for diagnostic precipitation is investigated over a range of conditions. It is found that, in general, two substeps are required for numerical stability and reasonably small time truncation errors using a time step of 20 min; however, substepping is only required for the precipitation microphysical processes rather than the entire scheme. A new numerical approach for the diagnostic rain and snow produces reasonable results compared to a benchmark simulation, especially at low vertical resolution. Part II of this study details results of the scheme in single-column and global simulations, including comparison with observations.

1. Introduction

The importance of cloud parameterization in general circulation models (GCMs) is well known (e.g., see review in Stephens 2005). Despite increased computing power, rather substantial simplifications still must be made for representing clouds in current GCMs due to the vast range of temporal and spatial scales associated with cloud processes. Thus, cloud parameterizations are a weak link in diagnosing interactions and feedbacks relevant to global climate change using GCMs (Stephens 2005).

While cloud microphysics must still be parameterized in higher-resolution cloud-resolving and mesoscale models, the large grid spacings of GCMs introduce additional difficulties related to cloud-dynamical-radiative interactions (convection in particular). GCMs address this problem in part by a scale separation between the convective and stratiform cloud systems. Convective clouds are treated by the convective parameterization(s), which typically employ a highly simplified treatment of the microphysics. Larger-scale, stratiform cloud systems are treated by the "stratiform" cloud microphysics parameterization, which typically employs a more detailed treatment of microphysics.

In stratiform cloud microphysics schemes, nearly all GCMs currently predict one or more species of cloud water. Precipitation water is generally treated diagnostically (e.g., Ghan and Easter 1992, hereafter GE92; Rotstayn 1997; Rasch and Kristjansson 1998), but it may be treated prognostically by retaining the time-dependent equations (e.g., Fowler et al. 1996). Simpler microphysics parameterizations diagnose the relative amounts of ice and liquid as a function of temperature (e.g., Del Genio 1996), while more complex parameterizations include separate prognostic equations for ice and liquid (e.g., Fowler et al. 1996; Lohmann and

* The National Center for Atmospheric Research is sponsored by the National Science Foundation.

Corresponding author address: Hugh Morrison, National Center for Atmospheric Research, Box 3000, Boulder, CO 80307-3000.
E-mail: morrison@ucar.edu

DOI: 10.1175/2008JCLI2105.1

© 2008 American Meteorological Society

Roeckner 1996; Rotstayn et al. 2000). In cold clouds (i.e., cloud temperatures below freezing), the fraction of cloud water present as liquid or ice has important implications for the cloud radiative properties, because droplets are typically smaller than cloud ice particles. In addition, precipitation occurs more readily in clouds containing substantial amounts of ice.

Microphysics parameterizations in GCMs are "bulk" schemes, meaning that they assume some functional form for the cloud particle size distribution(s) and predict one or more moments of the distribution, such as the mixing ratio. A recent improvement in bulk microphysics schemes has been the prediction of two moments of the particle size distribution (i.e., mixing ratio and number concentration). Prediction of both number and mixing ratio increases the degrees of freedom and potentially improves calculation of the microphysical processes relative to using one-moment schemes predicting mixing ratio only. Two-moment schemes have been used fairly extensively in cloud-resolving and mesoscale models (e.g., Ferrier 1994; Meyers et al. 1997; Khairoutidnov and Kogan 2000; Seifert and Beheng 2001; Morrison and Pinto 2005; Milbrandt and Yau 2005; Morrison and Grabowski 2007; Phillips et al. 2007). Simplified two-moment schemes have also been developed for GCMs (e.g., Ghan et al. 1997; Lohmann et al. 1999; Ming et al. 2007). A motivation for the development of two-moment schemes has been the recent focus on indirect aerosol effects, that is, the impact of atmospheric aerosols on clouds and hence radiative transfer (e.g., Twomey 1977; Albrecht 1989). The prediction of both number concentration and mixing ratio allows the effective radius to evolve in a much more realistic manner compared to using one-moment schemes that specify the cloud particle number concentration or effective radius and allow for more robust interaction between clouds and aerosols.

In this paper, we introduce a new two-moment parameterization for stratiform cloud microphysics and precipitation in the Community Atmosphere Model, version 3 (CAM3) developed at the National Center for Atmospheric Research (NCAR). CAM3 is the atmospheric component of the Community Climate System Model (CCSM3). The new scheme includes prognostic variables for the cloud droplet and cloud ice mixing ratios and number concentrations, while precipitation is treated diagnostically.

The new parameterization seeks the following:

1) a more flexible, self-consistent, physically based treatment of cloud physics;
2) a reasonable level of simplicity and computational efficiency;
3) treatment of both number concentration and mixing ratio of cloud particles to address indirect aerosol effects and cloud–aerosol interaction;
4) representation of precipitation number concentration, mass, and phase to better treat wet deposition and scavenging of aerosol and chemical species; and
5) the achievement of equivalent or better results relative to the current CAM3 parameterization when compared to observations.

The novel aspects of the scheme, relative to other two-moment schemes recently developed for GCMs (e.g., Ghan et al. 1997; Lohmann et al. 1999; Ming et al. 2007), are an explicit representation of subgrid cloud water distribution for calculation of the various microphysical process rates as well as the diagnostic two-moment treatment of rain and snow.

The goals of this paper are to document the new scheme and to examine in detail its numerical aspects. Part II of this study (Gettelman et al. 2008) presents single-column and global results using the new scheme, focusing on comparison with the control CAM3 scheme as well as observations. Part II also details results concerning cloud and precipitation particle number concentration and size. The paper is organized as follows: section 2 provides an overview of the scheme; section 3 gives a detailed description of the microphysical processes; numerical tests are described in section 4; and a summary and conclusions are given in section 5.

2. Overview of the microphysics scheme

The two-moment scheme is based loosely on the approach of Morrison et al. (2005). This scheme predicts the number concentrations (N_c, N_i) and mixing ratios (q_c, q_i) of cloud droplets (subscript c) and cloud ice (subscript i). Hereafter, unless stated otherwise, the cloud variables N_c, N_i, q_c, and q_i represent grid-averaged values; prime variables represent mean in-cloud quantities (e.g., such that $N_c = F_{\rm cld} N_c'$, where $F_{\rm cld}$ is cloud fraction); and double prime variables represent local in-cloud quantities. The treatment of subgrid cloud variability is detailed in section 2a.

The cloud droplet and ice size distributions ϕ are represented by gamma functions:

$$\phi(D) = N_0 D^{\mu} e^{-\lambda D}, \tag{1}$$

where D is diameter, N_0 is the "intercept" parameter, λ is the slope parameter, and $\mu = 1/\eta^2 - 1$ is the spectra shape parameter; η is the relative radius dispersion of the size distribution. The parameter η for droplets is specified following Martin et al. (1994). Their observations of maritime versus continental warm stratocumulus have been approximated by the following $\eta - N_c''$ relationship:

$$\eta = 0.000\,571\,4 N_c'' + 0.2714, \quad (2)$$

where N_c'' has units of cm^{-3}. The upper limit for η is 0.577, corresponding with a N_c'' of 535 cm^{-3}. Note that this expression is uncertain, especially when applied to cloud types other than those observed by Martin et al. (1994). In the current version of the new scheme, $\mu = 0$ for cloud ice.

The spectral parameters N_0 and λ are derived from the predicted N'' and q'' and specified μ:

$$\lambda = \left[\frac{\pi\rho N''\Gamma(\mu+4)}{6q''\Gamma(\mu+1)}\right]^{(1/3)}, \quad (3)$$

$$N_0 = \frac{N''\lambda^{\mu+1}}{\Gamma(\mu+1)}, \quad (4)$$

where Γ is the Euler gamma function. Note that (3) and (4) assume spherical cloud particles with bulk density $\rho = 1000$ kg m^{-3} for droplets and $\rho = 500$ kg m^{-3} for cloud ice, following Reisner et al. (1998).

The effective radii for droplets and cloud ice needed by the radiative transfer scheme are obtained directly by dividing the third and second moments of the size distribution given by (1). After rearranging terms, this yields

$$r_e = \frac{\Gamma(\mu+4)}{2\lambda\Gamma(\mu+3)}. \quad (5)$$

The time evolution of q and N is determined by grid-scale advection, convective detrainment, turbulent diffusion, and several microphysical processes:

$$\frac{\partial N}{\partial t} + \frac{1}{\rho}\nabla\cdot[\rho\mathbf{u}N] = \left(\frac{\partial N}{\partial t}\right)_{\text{nuc}} + \left(\frac{\partial N}{\partial t}\right)_{\text{evap}} + \left(\frac{\partial N}{\partial t}\right)_{\text{auto}} + \left(\frac{\partial N}{\partial t}\right)_{\text{accr}} + \left(\frac{\partial N}{\partial t}\right)_{\text{accs}} + \left(\frac{\partial N}{\partial t}\right)_{\text{het}} + \left(\frac{\partial N}{\partial t}\right)_{\text{hom}} + \left(\frac{\partial N}{\partial t}\right)_{\text{mlt}} + \left(\frac{\partial N}{\partial t}\right)_{\text{sed}} + \left(\frac{\partial N}{\partial t}\right)_{\text{det}} + D(N), \quad (6)$$

$$\frac{\partial q}{\partial t} + \frac{1}{\rho}\nabla\cdot[\rho\mathbf{u}q] = \left(\frac{\partial q}{\partial t}\right)_{\text{cond}} + \left(\frac{\partial q}{\partial t}\right)_{\text{evap}} + \left(\frac{\partial q}{\partial t}\right)_{\text{auto}} + \left(\frac{\partial q}{\partial t}\right)_{\text{accr}} + \left(\frac{\partial q}{\partial t}\right)_{\text{accs}} + \left(\frac{\partial q}{\partial t}\right)_{\text{het}} + \left(\frac{\partial q}{\partial t}\right)_{\text{hom}} + \left(\frac{\partial q}{\partial t}\right)_{\text{mlt}} + \left(\frac{\partial q}{\partial t}\right)_{\text{sed}} + \left(\frac{\partial q}{\partial t}\right)_{\text{det}} + D(q), \quad (7)$$

where t is time, $\mathbf{u}$ is the 3D wind vector, ρ is the air density, and D is the turbulent diffusion operator. The symbolic terms on the right-hand side of (6) and (7) represent the grid-average microphysical source/sink terms for N and q. Note that the source/sink terms for q and N are considered separately for cloud water and ice (giving a total of four rate equations), but they are generalized here using (6) and (7) for conciseness. These terms include activation of cloud condensation nuclei or deposition/condensation-freezing nucleation on ice nuclei to form droplets or cloud ice (subscript nuc; N only); condensation/deposition (subscript cond; q only); evaporation/sublimation (subscript evap); autoconversion of cloud droplets and ice to form rain and snow (subscript auto); accretion of cloud droplets and ice by rain (subscript accr); accretion of cloud droplets and ice by snow (subscript accs); heterogeneous freezing of droplets to form ice (subscript het); homogeneous freezing of cloud droplets (subscript hom); melting (subscript mlt); sedimentation (subscript sed); and convective detrainment (subscript det). The formulations for these processes are detailed in section 3. Numerical aspects in solving (6) and (7) are detailed in section 4.

a. Subgrid cloud variability

Cloud water variability within the grid cell of a large-scale model is important because many microphysical processes vary nonlinearly with cloud water amount. For example, as pointed out by Pincus and Klein (2000), Rotstayn et al. (2000), and Larson et al. (2001), precipitation formation is highly nonlinear, resulting in potentially substantial biases if only the mean in-cloud cloud water is considered. As described by Tompkins (2002), a wide variety of probability density functions (PDFs) has been used in GCMs to represent cloud variability because of the difficulty in obtaining this information directly from observations at small scales. We view the PDF approach as more physically consistent than tuning individual microphysical processes such as autoconversion (as has been done often in previous studies) because 1) subgrid cloud water variability in terms of a PDF is a real physical quantity that can be obtained, at least in principle, from observations or high-resolution cloud models, and 2) the PDF approach for cloud water variability allows for a self-consistent treatment of the impact of this variability on the various microphysical processes.

Subgrid variability is considered for cloud water but neglected for cloud ice and precipitation at present; furthermore, we neglect subgrid variability of droplet number concentration for simplicity. We focus on subgrid variability of cloud water because there is some empirical basis for the underlying distribution functions, as described below, and because cloud water microphysics is comparatively well understood at the process level compared with ice microphysics (parameterization of ice microphysics is complicated by uncertainties in crystal habit, diffusional growth rate, ice nucleation, aggregation efficiency, etc.). Here we assume that the PDF of in-cloud cloud water, $P(q_c'')$, follows a gamma distribution function based on observations of optical depth in marine boundary layer clouds (Barker 1996; Barker et al. 1996; Pincus et al. 1999):

$$P(q_c'') = \frac{q_c''^{\nu-1}\alpha^{\nu}}{\Gamma(\nu)} e^{-\alpha q_c''}, \tag{8}$$

where $\nu = 1/\sigma^2$; σ^2 is the relative variance (i.e., variance divided by $q_c'^2$), and $\alpha = \nu/q_c'$ (q_c' is the mean in-cloud cloud water mixing ratio). Note that this PDF is applied to all cloud types treated by the stratiform cloud scheme; the appropriateness of such a PDF for stratiform cloud types other than marine boundary layer clouds (e.g., deep frontal clouds) is uncertain given a lack of observations.

Satellite retrievals described by Barker et al. (1996) suggest that $\nu > 1$ in overcast conditions and $\nu \sim 1$ (corresponding to an exponential distribution) in broken stratocumulus. It should be kept in mind that Barker et al. express variability in terms of cloud optical depth; thus, it depends on both r_e and q_c'' as well as cloud depth. They relate ν to the cloud fraction [see their Eq. (14)] but note that the "conditional variance of ν for a given cloud fraction is substantial." They also stress scale dependence of ν and caution against using this relationship between ν and cloud fraction in models with a horizontal resolution much different from 60 km. Furthermore, the applicability of such a relationship to cloud types other than boundary layer clouds is uncertain. Despite these uncertainties, the key point is that our representation of subgrid cloud variability has at least some empirical basis (especially for boundary layer clouds) and provides a consistent treatment of the microphysical processes without the arbitrary tuning of individual processes. Significant efforts will be required in the future to better relate subgrid cloud water variability to observations for the range of stratiform cloud types. For the simulations presented in Part II, the model assumes a constant $\nu = 1$ for simplicity, although sensitivity to the subgrid cloud water variability is discussed.

TABLE 1. Enhancement factor E of droplet microphysical process rates due to subgrid variability of cloud water, for different values of inverse relative variance, ν. The values of ν of 0.5, 1, and 8 represent the mean values found by Barker et al. (1996) for low cloud fraction (<0.2), broken stratocumulus, and overcast conditions, respectively (although Barker et al. noted significant scatter in values of ν in overcast conditions).

	Inverse relative variance (ν)		
	0.5	1	8
Process rate	Enhancement factor (E)		
Autoconversion	6.08	3.22	1.23
Immersion freezing	3.00	2.00	1.13
Accretion by rain	1.13	1.07	1.01

A major advantage of using gamma functions to represent subgrid variability of cloud water is that the grid-average microphysical process rates can be derived in a straightforward manner. For any generic local microphysical process rate $M_p = xq_c''^y$, replacing q_c'' with $P(q_c'')$ from (8) and integrating over the PDF yields a mean in-cloud process rate of

$$M_p' = x\frac{\Gamma(\nu + y)}{\Gamma(\nu)\nu^y} q_c'^y. \tag{9}$$

Thus, each cloud water microphysical process rate in (6) and (7) is multiplied by a factor of

$$E = \frac{\Gamma(\nu + y)}{\Gamma(\nu)\nu^y}. \tag{10}$$

The impact of different values of E on the various microphysical processes for different ν is shown in Table 1. Subgrid cloud water variability has a large impact on autoconversion and less of an impact on the other processes, especially accretion of cloud water by rain. As expected, E increases with an increase in relative variance (decrease in ν).

Ideally, the subgrid distribution of cloud water should be consistent with the subgrid variance of total water, such as in the scheme of Tompkins (2002). Future work will improve the consistency between the subgrid treatment of the microphysics and the subgrid treatment of the other aspects of the thermodynamics such as the total water. This treatment could also be easily extended to include cloud ice and precipitation, although difficulties might arise if cross correlations among different cloud/precipitation species were considered. Furthermore, subgrid variability at GCM scales for these species is even less well understood than it is for cloud water, but the development of new satellite remote sensing tools (Stephens et al. 2002) should help to address this issue.

b. Diagnostic treatment of precipitation

As described by GE92, diagnostic treatment of precipitation allows for a longer time step, because prognostic precipitation is constrained by the Courant criterion for sedimentation. Furthermore, the neglect of horizontal advection of precipitation in the diagnostic approach is reasonable given the large grid spacing (~100 km) and long time step (~15–40 min) of GCMs. A unique aspect of this scheme is the diagnostic treatment of both precipitation mixing ratio q_p and number concentration N_p. Considering only the vertical dimension, the grid-scale time rates of change of q_p and N_p are

$$\frac{\partial q_p}{\partial t} = \frac{1}{\rho}\frac{\partial (V_q \rho q_p)}{\partial z} + S_q, \tag{11}$$

$$\frac{\partial N_p}{\partial t} = \frac{1}{\rho}\frac{\partial (V_N \rho N_p)}{\partial z} + S_N, \tag{12}$$

where z is height, V_q and V_N are the mass- and number-weighted terminal fall speeds, respectively, and S_q and S_N are the grid-mean source/sink terms for q_p and N_p, respectively:

$$S_q = \left(\frac{\partial q_p}{\partial t}\right)_{\text{auto}} + \left(\frac{\partial q_p}{\partial t}\right)_{\text{accw}} + \left(\frac{\partial q_p}{\partial t}\right)_{\text{acci}} + \left(\frac{\partial q_p}{\partial t}\right)_{\text{het}} + \left(\frac{\partial q_p}{\partial t}\right)_{\text{hom}} + \left(\frac{\partial q_p}{\partial t}\right)_{\text{mlt}} + \left(\frac{\partial q_p}{\partial t}\right)_{\text{evap}} + \left(\frac{\partial q_p}{\partial t}\right)_{\text{coll}}, \tag{13}$$

$$S_N = \left(\frac{\partial N_p}{\partial t}\right)_{\text{auto}} + \left(\frac{\partial N_p}{\partial t}\right)_{\text{het}} + \left(\frac{\partial N_p}{\partial t}\right)_{\text{hom}} + \left(\frac{\partial N_p}{\partial t}\right)_{\text{mlt}} + \left(\frac{\partial N_p}{\partial t}\right)_{\text{evap}} + \left(\frac{\partial N_p}{\partial t}\right)_{\text{self}} + \left(\frac{\partial N_p}{\partial t}\right)_{\text{coll}}. \tag{14}$$

The symbolic terms on the right-hand sides of (13) and (14) are autoconversion (subscript auto), accretion of cloud water (subscript accw), accretion of cloud ice (subscript acci), heterogeneous freezing (subscript het), homogeneous freezing (subscript hom), melting (subscript mlt), evaporation (subscript evap), self-collection (subscript self; collection of rain drops by other rain drops, or snow crystals by other snow crystals; N_p only), and collection of rain by snow (subscript coll). Formulations for these processes are described in section 3.

In the diagnostic treatment, $(\partial q_p/\partial t) = 0$ and $(\partial N_p/\partial t) = 0$. This allows (11) and (12) to be expressed as a function of z only. The q_p and N_p are therefore determined by discretizing and numerically integrating (11)–(12) downward from the top of the model atmosphere, following GE92:

$$\rho_{a,k} V_{q,k} q_{p,k} = \rho_{a,k+1} V_{q,k+1} q_{p,k+1} + \frac{1}{2}[\rho_{a,k} S_{q,k} \Delta z_k + \rho_{a,k+1} S_{q,k+1} \Delta z_{k+1}], \tag{15}$$

$$\rho_{a,k} V_{N,k} N_{p,k} = \rho_{a,k+1} V_{N,k+1} N_{p,k+1} + \frac{1}{2}[\rho_{a,k} S_{N,k} \Delta z_k + \rho_{a,k+1} S_{N,k+1} \Delta z_{k+1}], \tag{16}$$

where k is the vertical level (increasing with height, i.e., $k + 1$ is the next vertical level above k). Because $V_{q,k}$, $S_{q,k}$, $V_{N,k}$, and $S_{N,k}$ depend on $q_{p,k}$ and $N_{p,k}$, (15) and (16) must be solved by iteration or some other method. The approach of GE92 uses values of $q_{p,k}$ and $N_{p,k}$ from the previous time step as provisional estimates to calculate $V_{q,k}$, $V_{N,k}$, $S_{p,k}$, and $S_{N,k}$. "Final" values of $q_{p,k}$ and $N_{p,k}$ are calculated from these values of $V_{q,k}$, $V_{N,k}$, $S_{q,k}$, and $S_{N,k}$ using (15) and (16). Here we employ another method that obtains provisional values of $q_{p,k}$ and $N_{p,k}$ from (15) and (16), assuming $V_{q,k} \sim V_{q,k+1}$ and $V_{N,k} \sim V_{N,k+1}$. It is also assumed that all source/sink terms in $S_{q,k}$ and $S_{N,q}$ can be approximated by the values at $k + 1$, except for the autoconversion, which can be obtained directly at the k level because it does not depend on $q_{p,k}$ or $N_{p,k}$. If there is no precipitation flux from the level above, then the provisional $q_{p,k}$ and $N_{p,k}$ are calculated using autoconversion at the k level in $S_{q,k}$ and $S_{N,k}$; $V_{q,k}$ and $V_{N,k}$ are estimated assuming newly formed rain and snow particles have fall speeds of 0.45 m s^{-1} for rain and 0.36 m s^{-1} for snow. The two approaches are tested in section 4.

Rain and snow are considered separately, and both may occur simultaneously in supercooled conditions (hereafter subscript p for precipitation is replaced by subscripts r for rain and s for snow). The rain/snow particle size distributions are given by (1), with the shape parameter $\mu = 0$, resulting in Marshall–Palmer (exponential) size distributions. The size distribution parameters λ and N_0 are similarly given by (3)–(4) with $\mu = 0$. The bulk particle density [parameter ρ in (3)] is $\rho = 1000$ kg m^{-3} for rain and $\rho = 100$ kg m^{-3} for snow, following Reisner et al. (1998).

c. Cloud and precipitation particle terminal fall speeds

The mass- and number-weighted terminal fall speeds for all cloud and precipitation species are obtained by integration over the particle size distributions with appropriate weighting by number concentration or mixing ratio:

$$V_N = \frac{\int_0^\infty \left(\frac{\rho_a}{\rho_{a0}}\right)^{0.54} aD^b \phi(D)\, dD}{\int_0^\infty \phi(D)\, dD} = \frac{\left(\frac{\rho_a}{\rho_{a0}}\right)^{0.54} a\Gamma(1 + b + \mu)}{\lambda^b \Gamma(\mu + 1)}, \tag{17}$$

$$V_q = \frac{\int_0^\infty \frac{\pi\rho}{6}\left(\frac{\rho_a}{\rho_{a0}}\right)^{0.54} aD^{b+3} \phi(D)\, dD}{\int_0^\infty \frac{\pi\rho}{6} D^3 \phi(D)\, dD} = \frac{\left(\frac{\rho_a}{\rho_{a0}}\right)^{0.54} a\Gamma(4 + b + \mu)}{\lambda^b \Gamma(\mu + 4)}, \tag{18}$$

where ρ_{a0} is the reference air density at STP and a and b are empirical coefficients in the diameter–fall speed relationship $V = aD^b$, where V is the terminal fall speed for an individual particle with diameter D. The air density correction factor is from Heymsfield et al. (2007). The V_N and V_q are limited to maximum values of 9.1 m s^{-1} for rain and 1.2 m s^{-1} for snow. The a and b coefficients for each hydrometeor species are given in Table 2. Note that for cloud water fall speeds, subgrid variability of q is considered by appropriately multiplying the V_N and V_q by the factor E given by (10).

3. Formulations for the microphysical processes

a. Activation of cloud droplets

Activation of cloud droplets, $(\partial N_c/\partial t)_{\text{nuc}}$, occurs on a multimodal lognormal aerosol size distribution based on the scheme of Abdul-Razzak and Ghan (2000). Activation of cloud droplets occurs if N_c decreases below the number of active cloud condensation nuclei diagnosed as a function of aerosol chemical and physical parameters, temperature, and vertical velocity (see Abdul-Razzak and Ghan 2000) and if liquid condensate is present. We use the existing N_c as a proxy for the number of aerosols previously activated as droplets because the actual number of activated aerosols is not tracked as a prognostic variable from time step to time step (for coupling with prescribed aerosol scheme as is done in Part II). This approach is similar to that of Lohmann et al. (1999). Because local rather than grid-scale vertical velocity is needed for calculating droplet activation, a subgrid vertical velocity w' is derived from the turbulent diffusion coefficient following Morrison et al. (2005):

$$w' = \frac{K_d}{l_c}, \tag{19}$$

where K_d is the turbulent diffusion coefficient (the diffusion coefficient for heat is used here) and $l_c = 30$ m is the mixing length. Note that mesoscale sources of w' are neglected (e.g., orography, gravity waves). In regions with weak turbulent diffusion, a minimum subgrid vertical velocity of 10 cm s^{-1} is assumed. Some models use the value of w' at cloud base to determine droplet activation in the cloud layer (e.g., Lohmann et al. 1999); however, because of coarse vertical and horizontal resolution and difficulty in defining the cloud base height in GCM's, we apply the w' calculated for a given layer to the droplet activation for that layer. Note that the droplet number may locally exceed the number activated for a given level due to advection of N_c. Some models implicitly assume that the time scale for droplet activation over a cloud layer is equal to the model time

TABLE 2. Fall speed parameters for the cloud and precipitation species.

Species	a parameter	b parameter	Reference
Cloud water	3×10^7 m^{1-b} s^{-1}	2	Ikawa and Saito (1990)
Cloud ice	700 m^{1-b} s^{-1}	1	Ikawa and Saito (1990)
Rain	841.997 m^{1-b} s^{-1}	0.8	Liu and Orville (1969)
Snow	11.72 m^{1-b} s^{-1}	0.41	Locatelli and Hobbs (1974)

step (e.g., Lohmann et al. 1999), which could enhance sensitivity to the time step. This time scale can be thought of as the time scale for recirculation of air parcels to regions of droplet activation (i.e., cloud base), similar to the time scale for large eddy turnover; here we assume an activation time scale of 20 min.

b. Primary ice nucleation

Nucleation of cloud ice by deposition/condensation-freezing modes, $(\partial N_i/\partial t)_{\text{nuc}}$, is calculated by assuming the ice nuclei concentration active in these modes, N_{IN} (in units of L^{-1}), is a function of temperature, T, following Cooper (1986):

$$N_{\text{IN}} = 0.005 \exp[0.304(T_0 - T)], \tag{20}$$

where $T_0 = 273.15$ K. Currently, in the new scheme, N_{IN} is not directly related to the aerosol characteristics (e.g., concentration of dust aerosols), although recent work (Khvorostyanov and Curry 2005; Kärcher and Lohmann 2002, 2003; Liu et al. 2007) has begun to address this issue. Because the Cooper ice nuclei concentrations are unreasonably large when extrapolated to very cold temperatures, the number concentration is limited here to the value calculated at −35°C (209 L^{-1}). The N_{IN} is assumed to be constant for a given temperature; deposition/condensation freezing nucleation occurs if N_i decreases below this value and $T < -5$°C. Similar to the droplet activation parameterization, the calculation of ice nucleation rate assumes a time scale of 20 min. Note that homogeneous freezing of haze aerosols (e.g., Liu et al. 2007) is not explicitly considered in the present version of the scheme. Ice multiplication via rime splintering (Hallet and Mossop 1974) or other processes is also neglected.

c. Condensation/deposition of cloud water and ice

The net grid-average evaporation/condensation rate of cloud water and ice (condensation minus evaporation), Q, is given by the fractional cloud closure scheme of Zhang et al. (2003). Net condensation occurs when $Q > 0$ (and net evaporation when $Q < 0$). This scheme provides a link between changes in cloud fraction and changes in total condensate and assumes that the grid-scale saturation mixing ratio $q_s(T)$ is a weighted average of the ice and water saturation mixing ratios that varies as a function of temperature. The partitioning of condensation rate between liquid and ice in Zhang et al. (2003) follows Rasch and Kristjansson (1998) as a linear function of temperature. This partitioning is modified here to include the Bergeron–Findeisen process, similar to the approach of Rotstayn et al. (2000). The local (in-cloud) deposition rate of water vapor onto cloud ice A is given by

$$A = \frac{(q_v^* - q_{\text{vi}}^*)}{\Gamma_p \tau}, \tag{21}$$

where q_v^* is the in-cloud water vapor mixing ratio, q_{vi}^* is the in-cloud vapor mixing ratio at ice saturation, $\Gamma_p = 1 + (L_s/c_p)(dq_{\text{vi}}/dT)$ is the psychrometric correction to account for the release of latent heat, L_s is the latent heat of sublimation, c_p is the specific heat at constant pressure, (dq_{vi}/dT) is the change of ice saturation vapor pressure with temperature, and the supersaturation relaxation time scale associated with ice deposition is given by

$$\tau = 2\pi N_{0i} \rho_a D_v \lambda_i^{-2}, \tag{22}$$

where D_v is the diffusivity of water vapor in air. Here, it is assumed that q_{vi}^* is equal to the ice saturation mixing ratio at the grid-scale temperature. In regions containing liquid, it is assumed that q_v^* is equal to the vapor mixing ratio at water saturation, q_{vs}. Assuming that Q and τ are evenly distributed within the cloudy portion of the grid cell, if the local cloud ice deposition rate A (assuming $q_v^* = q_{\text{vs}}$) exceeds Q, then the new condensate from Q forms as cloud ice. Correspondingly, if $A < Q$, then the local "excess" condensate given by $Q - A$ forms as cloud water. For temperatures below −40°C, it is assumed that any new liquid condensate is instantaneously converted to cloud ice by homogeneous freezing. Thus, the fraction of Q converted to ice is given by $F_{\text{ice}} = \min(A/Q, 1)$, when $Q > 0$ and $-40°\text{C} < T < 0°\text{C}$. It follows that the fraction of Q representing droplet condensation is $F_{\text{liq}} = \max(1 - A/Q, 0)$, when $Q > 0$ and $-40°\text{C} < T < 0°\text{C}$. For $T < -40°\text{C}$, $F_{\text{ice}} = 1$ and $F_{\text{liq}} = 0$; for $T > 0°\text{C}$, $F_{\text{ice}} = 0$ and $F_{\text{liq}} = 1$.

The growth of ice through the Bergeron process may also deplete *existing* cloud liquid water if $A > Q$. Thus, the total grid-scale condensation growth rate of ice is

$$\left(\frac{\partial q_i}{\partial t}\right)_{\text{cond}} = \min\left(F_{\text{cld}} A, F_{\text{cld}} Q + \frac{q_c}{\Delta t}\right), \quad Q > 0, \tag{23}$$

where F_{cld} is the cloud fraction and Δt is the model time step. The grid-scale condensation rate of cloud water is

$$\left(\frac{\partial q_c}{\partial t}\right)_{\text{cond}} = \max\left[F_{\text{cld}} Q - \left(\frac{\partial q_i}{\partial t}\right)_{\text{cond}}, 0\right], \quad Q > 0. \tag{24}$$

d. Evaporation/sublimation of cloud water and ice

If $Q < 0$, then it is assumed that droplets preferentially evaporate before sublimation of cloud ice occurs. If $F_{\text{cld}} Q < -q_c/\Delta t$, then ice sublimation occurs if cloud

ice is present. Thus, the grid-scale evaporation rate of cloud water (excluding sedimentation from cloudy into clear regions) is

$$\left(\frac{\partial q_c}{\partial t}\right)_{\text{evap}} = \max\left(F_{\text{cld}}Q, -\frac{q_c}{\Delta t}\right), \quad Q < 0. \tag{25}$$

The grid-scale sublimation rate of cloud ice (excluding sedimentation from cloudy into clear regions) is

$$\left(\frac{\partial q_i}{\partial t}\right)_{\text{evap}} = \max\left[F_{\text{cld}}Q - \left(\frac{\partial q_c}{\partial t}\right)_{\text{evap}}, -\frac{q_i}{\Delta t}\right], \quad Q < 0. \tag{26}$$

The reduction of grid-scale cloud water and ice number concentrations due to evaporation/sublimation, $(\partial N_c/\partial t)_{\text{evap}}$ and $(\partial N_i/\partial t)_{\text{evap}}$, is proportional to the corresponding reduction of mixing ratio.

e. Conversion of cloud water to rain

Autoconversion of cloud droplets and accretion of cloud droplets by rain is given by a version of the Khairoutdinov and Kogan (2000) scheme that is modified here to account for subgrid variability of cloud water within the cloudy part of the grid cell, as described previously in section 2a. Note that the Khairoutdinov and Kogan scheme was originally developed for boundary layer stratocumulus but is applied here to all stratiform cloud types.

The grid-mean autoconversion and accretion rates are found by replacing the q_c in Eqs. (29) and (33) of Khairoutdinov and Kogan (2000) with $P(q_c'')$ given by (8) here, integrating the resulting expressions over the cloud water PDF, and multiplying by the cloud fraction. This yields

$$\left(\frac{\partial q_c}{\partial t}\right)_{\text{auto}} = -F_{\text{cld}}\frac{\Gamma(\nu + 2.47)}{\Gamma(\nu)\nu^{2.47}}1350 q_c'^{2.47} N_c'^{-1.79}, \tag{27}$$

$$\left(\frac{\partial q_c}{\partial t}\right)_{\text{accr}} = -F_{\text{cld}}\frac{\Gamma(\nu + 1.15)}{\Gamma(\nu)\nu^{1.15}}67(q_c' q_r')^{1.15}. \tag{28}$$

The changes in q_r due to autoconversion and accretion are given by $(\partial q_r/\partial t)_{\text{auto}} = -(\partial q_c/\partial t)_{\text{auto}}$ and $(\partial q_r/\partial t)_{\text{accr}} = -(\partial q_c/\partial t)_{\text{accr}}$. The changes in N_c and N_r due to autoconversion and accretion, $(\partial N_c/\partial t)_{\text{auto}}$, $(\partial N_r/\partial t)_{\text{auto}}$, $(\partial N_c/\partial t)_{\text{accr}}$, are derived from Eqs. (32) and (35) in Khairoutdinov and Kogan (2000). Because accretion is nearly linear with respect to q_c, subgrid variability of cloud water is much less important for accretion than it is for autoconversion.

Note that in the presence of a precipitation flux into the layer from above, new drizzle drops formed by cloud droplet autoconversion would be accreted rapidly by existing precipitation particles (rain or snow) given collection efficiencies near unity for collision of drizzle with rain or snow (e.g., Pruppacher and Klett 1997). This may be especially important in models with low vertical resolution, because they cannot resolve the rapid growth of precipitation that occurs over distances much less than the vertical grid spacing. Thus, if the rain or snow mixing ratio in the next level above is greater than 10^{-6} g kg^{-1}, we assume that autoconversion produces an increase in rain mixing ratio but not number concentration (because the newly formed drops are assumed to be rapidly accreted by the existing precipitation). Otherwise, autoconversion results in a source of both rain mixing ratio and number concentration.

f. Conversion of cloud ice to snow

The autoconversion of cloud ice to form snow is calculated by integration of the cloud ice mass- and number-weighted size distributions greater than some specified threshold size, and transferring the resulting mixing ratio and number into the snow category over some specified time scale, similar to Ferrier (1994). The grid-scale changes in q_i and N_i due to autoconversion are

$$\left(\frac{\partial q_i}{\partial t}\right)_{\text{auto}} = -F\frac{\pi\rho_i N_{0i}}{6\tau_{\text{auto}}}\left[\frac{D_{cs}^3}{\lambda_i} + \frac{3D_{cs}^2}{\lambda_i^2} + \frac{6D_{cs}}{\lambda_i^3} + \frac{6}{\lambda_i^4}\right]e^{-\lambda_i D_{cs}}, \tag{29}$$

$$\left(\frac{\partial N_i}{\partial t}\right)_{\text{auto}} = -F\frac{N_{0i}}{\lambda_i\tau_{\text{auto}}}e^{-\lambda_i D_{cs}}, \tag{30}$$

where $D_{cs} = 200$ μm is the threshold size separating cloud ice from snow, ρ_i is the bulk density of cloud ice, and $\tau_{\text{auto}} = 3$ min is the assumed autoconversion time scale. Note that this formulation assumes the shape parameter $\mu = 0$ for the cloud ice size distribution; a different formulation must be used for other values of μ. The changes in q_s and N_s due to autoconversion are given by $(\partial q_s/\partial t)_{\text{auto}} = -(\partial q_i/\partial t)_{\text{auto}}$ and $(\partial N_s/\partial t)_{\text{auto}} = -(\partial N_i/\partial t)_{\text{auto}}$.

Accretion of q_i and N_i by snow, $(\partial q_i/\partial t)_{\text{accs}}$, $(\partial N_i/\partial t)_{\text{accs}}$, and $(\partial q_s/\partial t)_{\text{acci}} = -(\partial q_i/\partial t)_{\text{accs}}$, are given by the continuous collection equation, following Lin et al. (1983), which assumes that the fall speed of snow $\gg$ cloud ice fall speed. The collection efficiency for collisions between cloud ice and snow is 0.1, following Reisner et al. (1998). Newly formed snow particles formed by cloud ice autoconversion are not assumed to be rapidly accreted by existing snowflakes, given aggregation efficiencies typically much less than unity (e.g., Field et al. 2006).

g. Other collection processes

The accretion of q_c and N_c by snow, $(\partial q_c/\partial t)_{\text{accs}}$, $(\partial N_c/\partial t)_{\text{accs}}$, and $(\partial q_s/\partial t)_{\text{accw}} = -(\partial q_c/\partial t)_{\text{accs}}$, are given by the continuous collection equation. The collection efficiency for droplet–snow collisions is a function of the Stokes number, following Thompson et al. (2004), and thus depends on droplet size. Self-collection of snow, $(\partial N_s/\partial t)_{\text{self}}$, follows Reisner et al. (1998) using an assumed collection efficiency of 0.1. Self-collection of rain, $(\partial N_r/\partial t)_{\text{self}}$, follows Beheng (1994). Collisions between rain and cloud ice, cloud droplets and cloud ice, and self-collection of cloud ice are neglected for simplicity. Collection of q_r and N_r by snow in subfreezing conditions, $(\partial q_r/\partial t)_{\text{coll}} = -(\partial q_s/\partial t)_{\text{coll}}$ and $(\partial N_r/\partial t)_{\text{coll}}$, is given by Ikawa and Saito (1990), assuming collection efficiency of unity.

h. Freezing of cloud droplets and rain

Heterogeneous freezing of cloud droplets and rain to form cloud ice and snow, respectively, occurs by immersion freezing following Bigg (1953), which has been utilized in previous microphysics schemes [e.g., Reisner et al. 1998, see their Eqs. (A22), (A.55), and (A.56); Morrison et al. 2005; Thompson et al. 2008). Here the freezing rates are integrated over the mass- and number-weighted cloud droplet and rain size distributions, and the impact of subgrid cloud water variability is included as described previously. While Lohmann (2002) suggests the possible importance on the global scale of heterogeneous ice formation via contact nucleation, it is neglected here for simplicity and because ice nuclei concentrations are not coupled to aerosol characteristics in the current version of the scheme. Homogeneous freezing of cloud droplets and rain to form cloud droplets and snow occurs instantaneously at −40°C.

i. Melting of cloud ice and snow

For simplicity, detailed formulations for heat transfer during melting of ice and snow are not included. Melting of cloud ice occurs instantaneously at 0°C. Melting of snow occurs instantaneously at +2°C. We have tested the sensitivity of both single-column and global results to changing the specified snow-melting temperature from +2° to 0°C and found no significant changes.

j. Evaporation/sublimation of precipitation

Evaporation of rain and sublimation of snow, $(\partial q_s/\partial t)_{\text{evap}}$ and $(\partial q_r/\partial t)_{\text{evap}}$, are given by diffusional mass balance in subsaturated conditions (Lin et al. 1983), including ventilation effects. Evaporation of precipitation occurs within the region of the grid cell containing precipitation but outside of the cloudy region. The fraction of the grid cell with evaporation of precipitation is therefore $F_{\text{pre}} - F_{\text{cld}}$, where F_{pre} is the precipitation fraction. Here, F_{pre} is calculated assuming maximum cloud overlap between vertical levels and neglecting tilting of precipitation shafts due to wind shear ($F_{\text{pre}} = F_{\text{cld}}$ at cloud top). The out-of-cloud water vapor mixing ratio is given by

$$q_{\text{clr}} = \frac{q_v - F_{\text{cld}} q_s(T)}{1 - F_{\text{cld}}}, \quad F_{\text{cld}} < 1, \tag{31}$$

where $q_s(T)$ is the in-cloud water vapor mixing ratio after bulk condensation/evaporation of cloud water and ice as described previously. As in the existing CAM3 microphysics parameterization, condensation/deposition onto rain/snow is neglected. Following Morrison et al. (2005), the evaporation/sublimation of N_r and N_s, $(\partial N_r/\partial t)_{\text{evap}}$ and $(\partial N_s/\partial t)_{\text{evap}}$, is proportional to the reduction of q_r and q_s during evaporation/sublimation.

k. Sedimentation of cloud water and ice

The time rates of change of q and N for cloud water and cloud ice due to sedimentation, $(\partial q_c/\partial t)_{\text{sed}}$, $(\partial q_i/\partial t)_{\text{sed}}$, $(\partial N_c/\partial t)_{\text{sed}}$, and $(\partial N_i/\partial t)_{\text{sed}}$, are calculated with a simple forward differencing scheme in the vertical dimension. Numerical stability for cloud water and ice sedimentation is ensured by substepping the time step, although these numerical stability issues are insignificant for cloud water and ice because of the low terminal fall speeds ($\ll 1$ m s^{-1}). We assume that the sedimentation of cloud water and ice results in evaporation/sublimation when the cloud fraction at the level above is larger than the cloud fraction at the given level (i.e., a sedimentation flux from cloudy into clear regions), with the evaporation/condensate rate proportional to the difference in cloud fraction between the levels.

l. Convective detrainment of cloud water and ice

The ratio of ice to total cloud condensate detrained from the convective parameterizations, F_{det}, is a linear function of temperature between −40° and −10°C; $F_{\text{det}} = 1$ at $T < -40$°C, and $F_{\text{det}} = 0$ at $T > -10$°C. Detrainment of number concentration is calculated by assuming a mean volume radius of 8 and 32 micron for droplets and cloud ice, respectively.

m. Numerical considerations

To ensure conservation of both q and N for each species, the magnitudes of the various sink terms are reduced if the provisional q and N are negative after stepping forward in time. This approach ensures critical

TABLE 3. Minimum and maximum mean number-weighted particle diameter (μm) allowed for the cloud and precipitation species.

Species	Minimum mean diameter	Maximum mean diameter
Cloud water	2	50
Cloud ice	10	400
Rain	20	500
Snow	10	2000

water and energy balances in the model and is similar to the approach employed in other bulk microphysics schemes (e.g., Reisner et al. 1998). Inconsistencies are possible because of the separate treatments for N and q, potentially leading to unrealistic mean cloud and precipitation particle sizes. For consistency, N is adjusted if necessary so that mean (number weighted) particle diameter ($=\Gamma(\mu + 1)/\lambda$) remains within a specified range of values for each species (Table 3). Limiting to a maximum mean diameter can be thought of as an implicit parameterization of particle breakup.

For the diagnostic precipitation, the source terms for q and N at a given vertical level are adjusted if necessary to ensure that the vertical integrals of the source terms (from that level to the model top) are positive. In other words, we ensure that at any given level, there isn't more precipitation removed (both in terms of mixing ratio and number concentration) than is available falling from above (this is also the case in the absence of any sources/sinks at that level). This check and possible adjustment of the precipitation and cloud water also ensures conservation of the total water and energy. Our simple adjustment procedure to ensure conservation could potentially result in sensitivity to the time step, although as described in section 3, time truncation errors are minimized with appropriate substepping.

Melting rates of cloud ice and snow are limited so that the temperature of the layer does not decrease below the melting point (i.e., in this instance an amount of cloud ice or snow is melted so that the temperature after melting is equal to the melting point). A similar approach is applied to ensure that homogeneous freezing does increase the temperature above homogeneous freezing threshold.

4. Numerical tests

The previous section presented differential equations [in time t and the three spatial coordinates x, y, z, see Eqs. (6) and (7)] for cloud water and ice mixing ratios and number concentrations. In addition, equations [in height z, see Eqs. (15) and (16) and discussion below] were presented for the diagnostic rain and snow mixing ratios and number concentrations. In this section, we focus on two key aspects of the numerical solution to these equations: 1) sensitivity to time step and 2) sensitivity to vertical resolution and the numerical procedure for calculating the diagnostic rain and snow mixing ratios and number concentrations. Broadly, our goal is to find the minimum level of sufficiency required to achieve an acceptable level of accuracy and numerical stability.

These tests are performed using a highly idealized one-dimensional framework with all physical processes turned off, except the cloud microphysics, and no vertical motion. This framework allows us to isolate issues directly related to the numerics of the scheme. Warm and cold conditions are used to test both the liquid and ice microphysics. The model setup is as follows: for the warm case, the atmosphere is initially isothermal with a temperature of 293 K. Between 550 and 800 mb, the initial relative humidity is 99% and a constant cooling rate of 6×10^{-4} K s^{-1} and a moistening rate of 6×10^{-8} s^{-1} are applied to induce cloud formation. Below 800 mb, the initial relative humidity is 80%. No temperature or moisture tendencies are applied below 800 mb, other than those produced by the cloud microphysics scheme. One-day integrations are performed. Although the vertical grid spacing in CAM3 ranges between about 20 and 90 mb, here we use a constant vertical grid spacing of 50 mb (except in the sensitivity tests as noted). The constant grid spacing helps to simplify the analysis, especially for the sensitivity tests varying the vertical grid spacing. For droplet activation, a single lognormal aerosol size distribution is considered, with a mean radius of 0.03 μm, a relative standard deviation of 1.5, and a concentration of 200 cm^{-3}. The subgrid vertical velocity is set to 1 m s^{-1}. Similar conditions are specified for the cold case, except the initial temperature is 233 K and the cooling and moistening rates between 550 and 800 mb are 2×10^{-4} K s^{-1} and 2×10^{-8} s^{-1}, respectively. In this case, the initial relative humidity is calculated with respect to ice. Note that for both the warm and the cold cases, the specified cooling and moistening rates correspond to rather strong forcing. Additional tests have been performed with weaker forcing to try to gauge the model performance over a wide range of conditions.

a. Sensitivity to time step

Forward-in-time numerical integration of the microphysics may be expected to produce significant time truncation errors as well as numerical instability given the long time step in CAM3 (20 min) and relatively

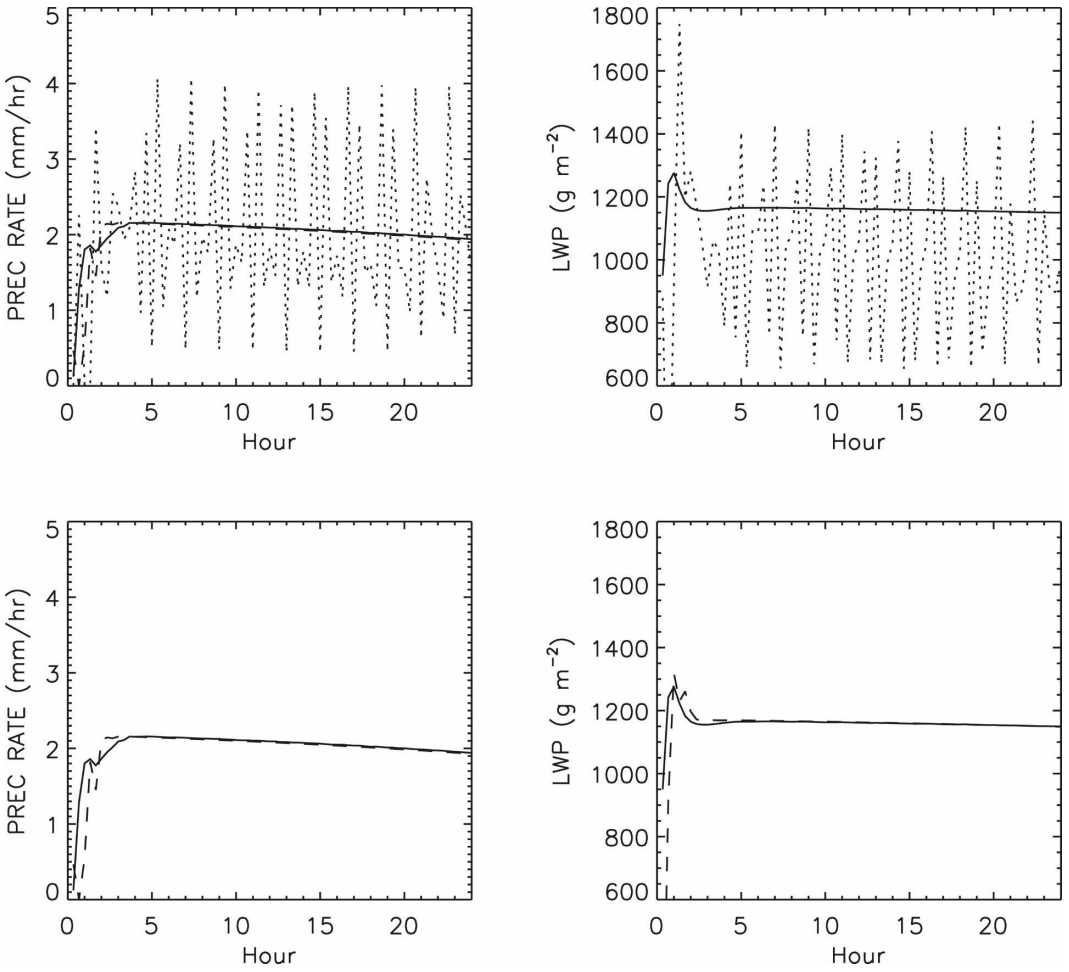

FIG. 1. (top) Time evolution of grid-mean surface precipitation rate and LWP using the 30-s benchmark time step (solid) and 1200-s time step with a single substep (dotted) and (bottom) using the 30-s benchmark time step (solid) and 1200-s time step with two substeps (dash).

short characteristic time scale for microphysical processes (<20 min). Thus, we explore substepping in time to address numerical instabilities and time truncation errors. Results are compared to a benchmark simulation that uses a 30-s time step; further reduction of this time step produces little change in the results.

To apply the substepping, the microphysics scheme is divided into three parts: 1) condensation/evaporation (including the Bergeron process), 2) precipitation microphysical processes, and 3) sedimentation of cloud water and ice. It is found that substepping over the precipitation processes is critical, while substepping over the other parts of the scheme has little impact. This likely reflects the faster time scale associated with precipitation microphysical processes compared with other aspects of the scheme. Hereafter, substepping refers to substepping of the precipitation microphysical processes only.

Figure 1 shows the time evolution of the grid-mean liquid water path (LWP) and surface precipitation rate (PREC) for the warm case using a 30-s time step (benchmark) and 1200-s CAM3 time step with either one or two substeps (note that hereafter "one substep" refers to calculation of all microphysical processes using the full model time step). Significant numerical instability occurs using a single substep. This instability is eliminated using two substeps; additional substeps have little impact. Despite the rather severe instabilities using a single substep, the mean LWP and PREC differ from benchmark by only 12% and 0.5%, respectively. Mean vertical profiles of in-cloud liquid water content, droplet number concentration, rainwater content, and rain number concentration are virtually identical between the benchmark and run with two substeps (Fig. 2). The mean vertical profiles from the run with a single substep are also generally similar to the benchmark,

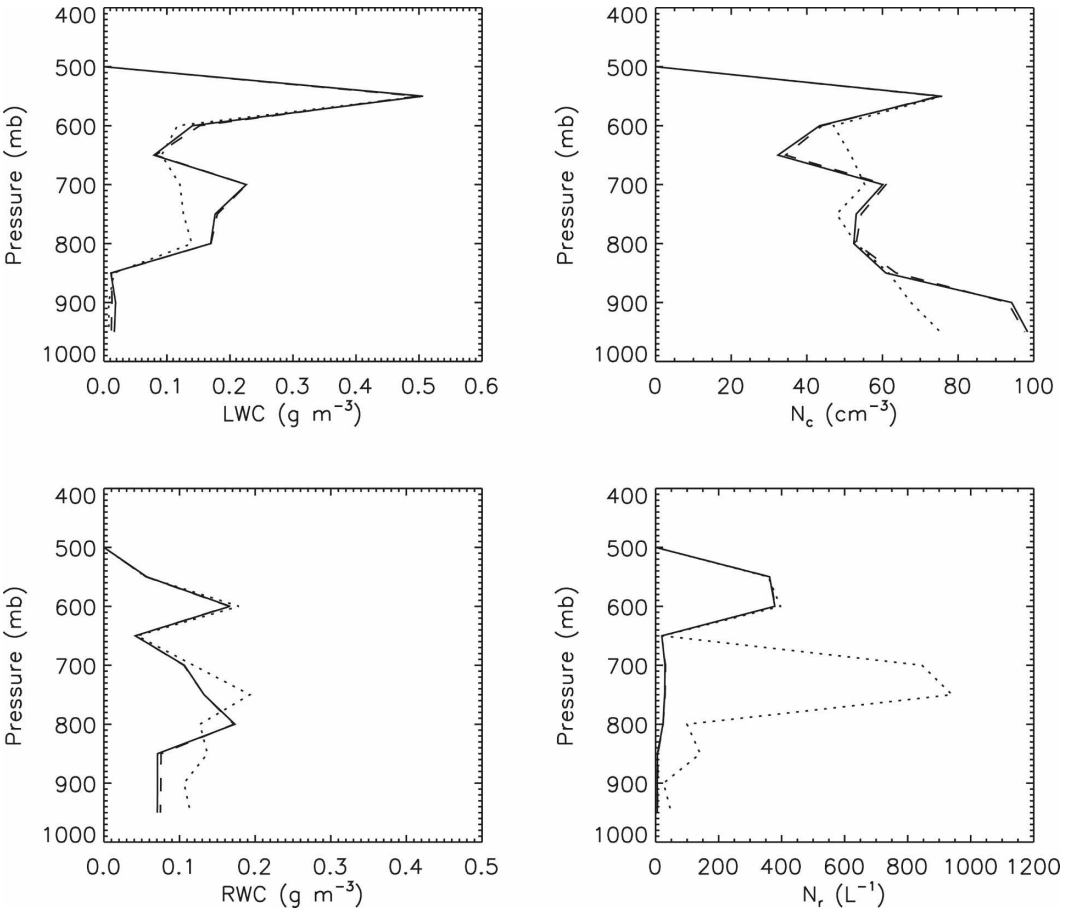

FIG. 2. Mean vertical profiles of in-cloud LWC, droplet number concentration (N_c), rainwater content (RWC), and rain number concentration (N_r), using the 30-s benchmark time step (solid), 1200-s time step with a single substep (dotted), and 1200-s time step with two substeps (dash). The averaging period includes hours 6–24 of the simulations.

except for the rain number concentration, which exhibits a large peak between 700 and 800 mb.

Results for the cold case in terms of grid-mean ice water path (IWP) and PREC are similar to the warm case, with the single substep resulting in numerical instability (Fig. 3). The mean vertical profiles of ice and snow water content are similar, while the profiles of cloud ice and snow number concentration are somewhat smaller using the single substep (Fig. 4). Additional tests (not shown) indicate that numerical stability is increased as the magnitude of the forcing (i.e., the applied temperature and moisture tendencies between 550 and 800 mb) is reduced, for both the warm and cold cases. In mixed-phase conditions, numerical instabilities occur using both one and twi substeps, but not three substeps (not shown). However, as detailed in Part II (Gettelman et al. 2008), global sensitivity tests of the scheme in CAM3 reveal little change using either two or three substeps, but significant differences between one and two substeps. Based on these results, combined with the findings presented here, we have decided to use two substeps in the standard version of the new scheme. Because the substepping involves precipitation microphysical processes only, the cost in terms of computational burden is not as significant as it might otherwise be. For the global results described in Part II, the new scheme produces an increase in total run time of 12%–14% relative to the Rasch and Kristjansson (1998) scheme in CAM3 using two substeps, although the code used for these runs was not yet optimized for efficiency.

b. Sensitivity to vertical resolution and numerical method for diagnostic precipitation

As detailed in section 2, additional numerical techniques must be employed when solving the discretized equations for diagnostic rain and snow number concen-

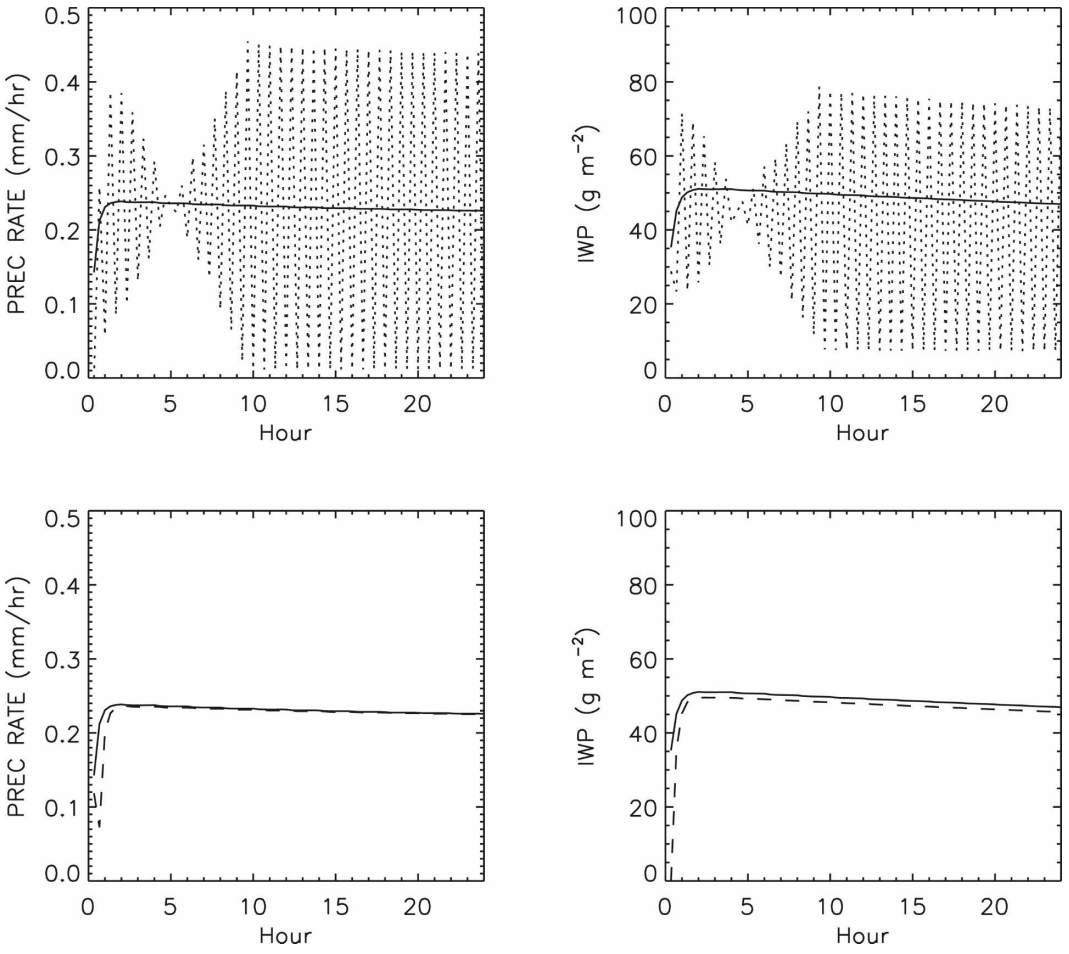

FIG. 3. (top) Time evolution of grid-mean surface precipitation rate and IWP using the 30-s benchmark time step (solid) and 1200-s time step with a single substep (dotted) and (bottom) using the 30-s benchmark time step (solid) and 1200-s time step with two substeps (dash).

tration as a function of height [Eqs. (15) and (16) in section 2]. Ghan and Easter (1992) solve the equation for diagnostic precipitation mixing ratio by using the mixing ratio at the previous time step to estimate the mean particle fall speed and source/sink terms. In section 2, we also describe a different procedure (hereafter the "new" method) that uses values at the next vertical level above to estimate the mean fall speed and source/sink terms for solving the diagnostic precipitation (see discussion below Eqs. (15) and (16) for details). Ideally, one would like to iterate until a reasonable level of convergence is reached for each time step, but unfortunately the large number of iterations required for convergence obviates this method except as a benchmark for testing the other approaches.

Results may also be sensitive to the vertical resolution given the sharp gradients of precipitation near cloud top. For the benchmark simulation, we increase the vertical resolution by a factor of 5 (resulting in a vertical grid spacing of 10 mb), and we iterate the solution to within 1% of convergence for each time step. All of the simulations use the standard CAM3 time step of 1200 s and two substeps as described in the previous subsection.

Figure 5 shows results in terms of grid-mean LWP and PREC for warm conditions using the benchmark setup or either the GE92 or new approaches and a vertical grid spacing of 50 mb. The GE92 method results in numerical instability that requires an increase in the number of substeps from two to three to mitigate. Our new approach is stable using two substeps but results in a mean LWP 13% larger than the benchmark. Note that in their paper, GE92 show significantly more sensitivity to vertical resolution (factor of 2 change in LWP with 4 times increase in resolution); it is not known whether our contrasting results reflect differences in the testing framework or in the parameterization of the various microphysical processes.

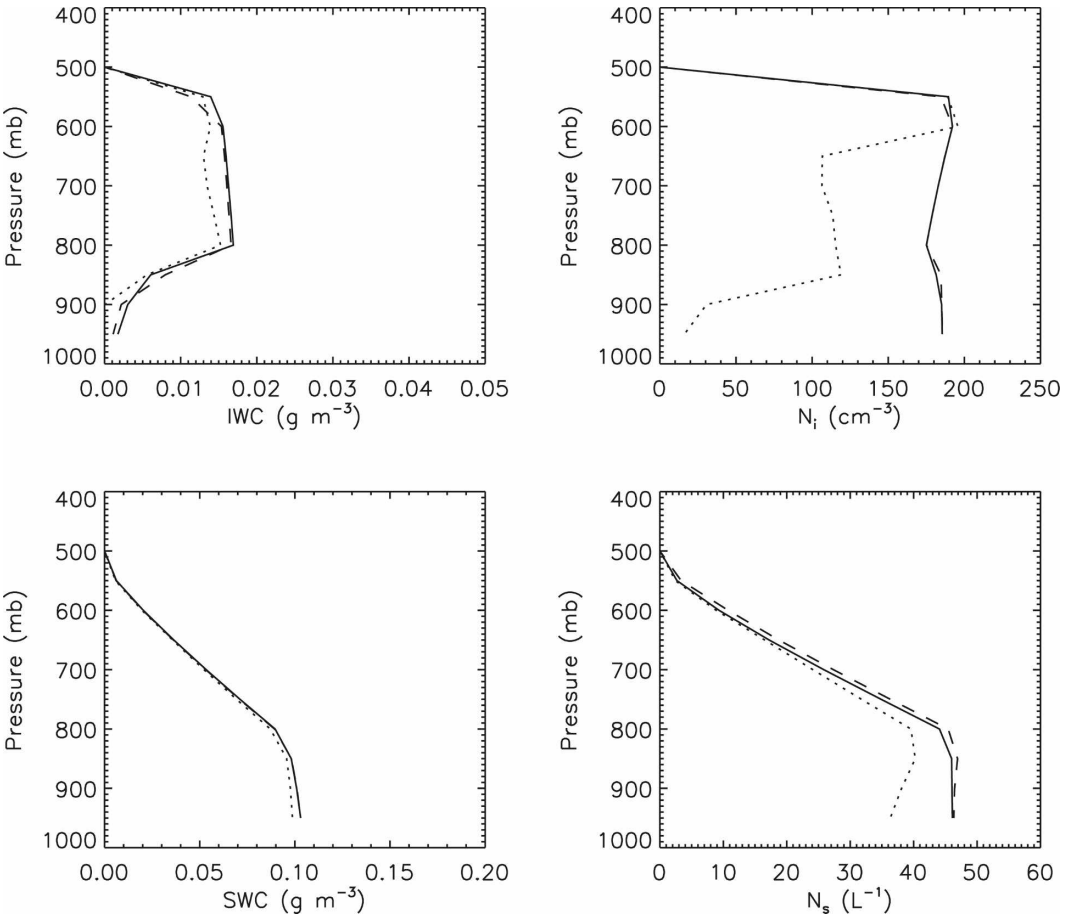

FIG. 4. Mean vertical profiles of in-cloud cloud IWC, cloud ice number concentration (N_i), snow water content (SWC), and snow number concentration (N_s), using 30-s benchmark time step (solid), 1200-s time step with a single substep (dotted), and 1200-s time step with two substeps (dash). The averaging period includes hours 6–24 of the simulations.

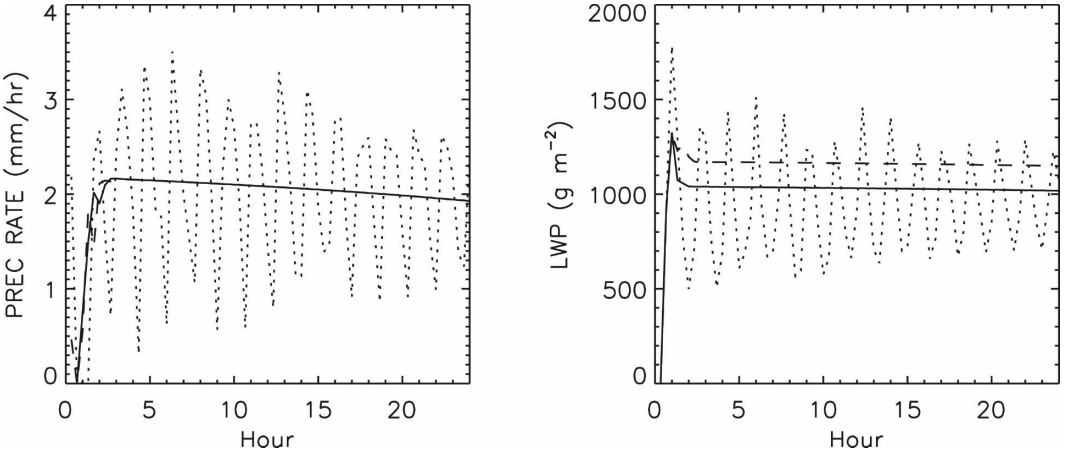

FIG. 5. Time evolution of grid-mean surface precipitation rate and LWP using the benchmark 10-mb vertical grid spacing and convergent iterative solution for diagnostic precipitation (solid), 50-mb vertical grid spacing and the GE92 approach for diagnostic precipitation (dotted), and 50-mb vertical grid spacing and the new approach (dash).

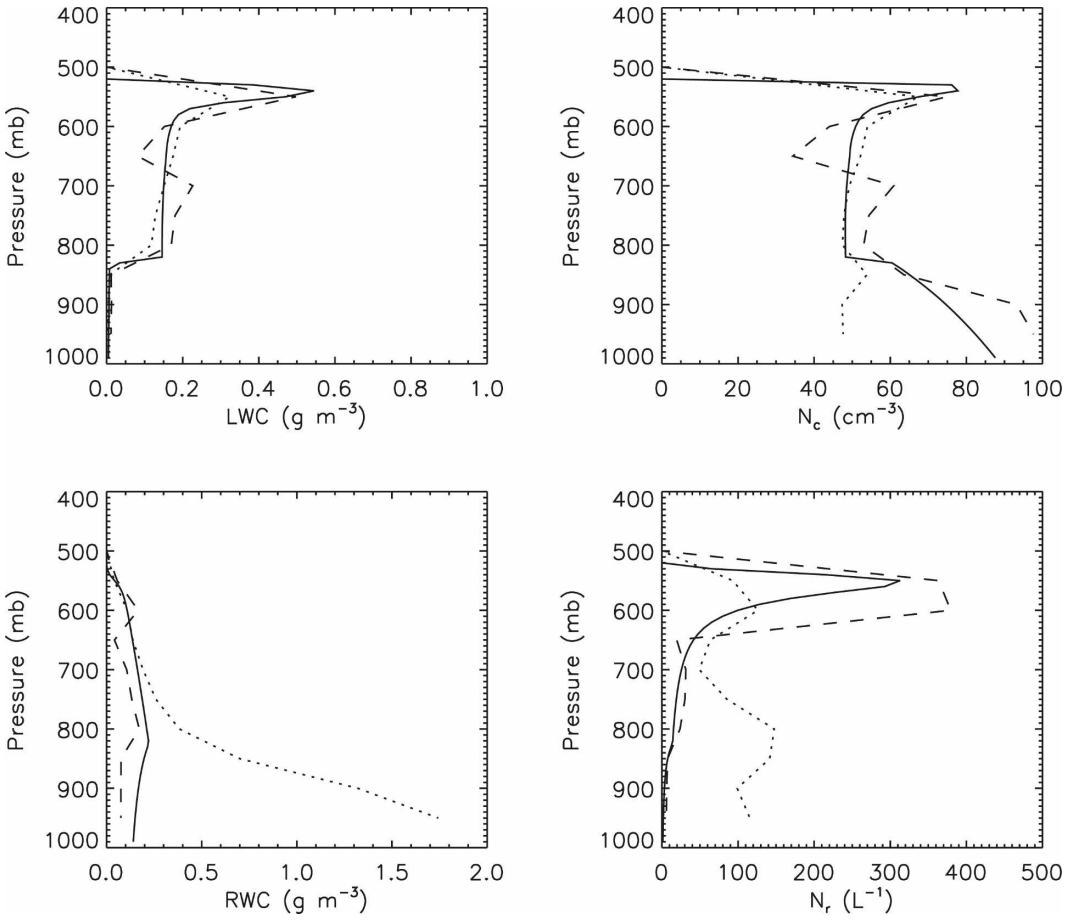

FIG. 6. Mean vertical profiles of in-cloud LWC, N_c, RWC, and N_r using the benchmark 10-mb vertical grid spacing and convergent iterative solution for diagnostic precipitation (solid), 50-mb vertical grid spacing and the GE92 approach for diagnostic precipitation (dotted), and 50-mb vertical grid spacing and the new approach (dash). The averaging period includes hours 6–24 of the simulations.

Mean vertical profiles of in-cloud liquid water content, droplet number concentration, rainwater content, and rain number concentration for the warm case are shown in Fig. 6. Profiles of liquid water content are similar among the runs, which is consistent with the overall similarity of LWP. The profiles of droplet number concentration are also similar. However, more significant differences are apparent for the rainwater content and number concentration. More specifically, the benchmark simulation shows a peak in the rainwater content of about 0.2 g m^{-3} occurring at 800 mb, and a sharp peak in rain number concentration near cloud top. The new approach captures these features fairly well, although the rain number concentration tends to be too large near its peak. In contrast, the GE92 approach produces a much different shape for the rain profiles, with maximum rainwater content exceeding 1.5 g m^{-3} near the surface, and maximum number concentration of 150 L^{-1} occurring near 800 mb. Note that most of the difference relative to the benchmark is due to use of the different methods in solving (15) and (16) rather than lower vertical resolution. A test using the convergent iterative solution, but with low vertical resolution (50-mb spacing), produces results that are similar to the benchmark, except that the peak rain number concentration is only about half as large (not shown). Differences among the various solutions are much smaller for the cold case.

As expected, differences between the approaches are reduced as the vertical resolution is increased. The numerical instability produced by the GE92 method with the baseline grid spacing (50 mb) is also substantially reduced with higher resolution, although instabilities are still present over the first several time steps. Overall, these results suggest that constraints on numerical stability and accuracy are dependent in a rather complex way on the various numerical aspects of the scheme tested here. Because of the improved results at

low resolution, especially in terms of numerical stability, we have chosen to use the new approach in the standard version of the new scheme rather than the GE92 method. Additional tests (not shown) indicate that differences between the GE92 and new procedures are diminished as the magnitude of the forcing (i.e., applied temperature and water vapor tendencies) is reduced.

5. Summary and conclusions

This paper has presented a new two-moment stratiform cloud microphysics scheme for the Community Atmosphere Model (CAM) GCM. Single-column and global results are presented in Part II (Gettelman et al. 2008), including a detailed comparison with observations. Prognostic variables include cloud droplet and cloud ice mixing ratios and number concentrations. Rain and snow mixing ratios and number concentrations are treated diagnostically. The parameterization of liquid microphysical processes has a strong physical basis at the process level. Instead, the major uncertainties concern the cloud "macrophysical" assumptions—cloud fraction, fractional condensation closure, and subgrid cloud water distribution. The parameterization of ice microphysics is less constrained at the process level than it is for liquid due to large uncertainties in crystal habit, diffusional growth rate, ice nucleation, aggregation efficiency, and so on. These uncertainties represent a major challenge to future parameterization development in both GCMs and higher-resolution models.

The key novel aspects of the scheme relative to other two-moment schemes that have been recently developed for GCMs (e.g., Ghan et al. 1997; Lohmann et al. 1999; Ming et al. 2007) are the explicit treatment of a subgrid cloud water distribution for calculation of the microphysical processes and the diagnostic two-moment representation (both mixing ratio and number concentration) of rain and snow. Both of these features improve the physical basis of the scheme. Although the treatment of the subgrid cloud water distribution is at present rather crude (a gamma distribution with constant relative variance), it is hoped that observations and cloud modeling studies will be able to better constrain these distributions in the future. We have also at present neglected subgrid distributions of cloud ice and precipitation; this important problem is also left for future work. Detailed evaluation of the diagnostic treatment of the rain and snow mixing ratios and number concentrations is given in Part II.

This paper also described testing of various numerical aspects of the scheme. We view this as a critical, if often overlooked issue in the development and testing of physical parameterizations in climate models. As the model physics are improved, care must be taken to minimize the impact of the numerical treatment, so that the solution is dependent on the improved physics. We focused this testing on two broad issues: 1) sensitivity to time step and 2) sensitivity to vertical resolution and the numerical solution for diagnostic precipitation. Substepping the precipitation microphysical processes in time was necessary to achieve numerical stability and minimize time-truncation errors, although in general only two substeps were required, except in mixed-phase conditions. Some sensitivity to vertical resolution was exhibited, although in our idealized tests the liquid water path and surface precipitation rate varied less than 13% with a fivefold decrease in the vertical grid spacing. Little sensitivity to vertical resolution was exhibited for the cold (ice only) case. The use of different methods to solve the equations for diagnostic precipitation had a significant impact on the mean vertical profiles of rainwater content and number concentration, as well as on the numerical stability; however, this impact was lessened as the vertical grid spacing was decreased. The idealized tests shown here used rather strong forcing in terms of the applied temperature and water tendencies. In general, it was found that numerical issues (e.g., instability and truncation errors) were less important as the magnitude of this forcing was decreased.

Acknowledgments. The work presented in this paper was supported by the National Science Foundation under Grant No. 0603539 and NASA MAP NNG06GBB1G. H. Morrison also acknowledges support from the National Center for Atmospheric Research Advanced Study Program. We thank P. Rasch and J. Dudhia for comments on the manuscript and valuable discussion.

REFERENCES

Abdul-Razzak, H., and S. J. Ghan, 2000: A parameterization of aerosol activation 2. Multiple aerosol types. *J. Geophys. Res.,* **105,** 6837–6844.

Albrecht, B. A., 1989: Aerosols, cloud microphysics, and fractional cloudiness. *Science,* **245,** 1227–1230.

Barker, H., 1996: A parameterization for computing grid-averaged solar fluxes for inhomogeneous marine boundary layer clouds. Part I: Methodology and homogeneous biases. *J. Atmos. Sci.,* **53,** 2289–2303.

——, B. A. Weilicki, and L. Parker, 1996: A parameterization for computing grid-averaged solar fluxes for inhomogeneous marine boundary layer clouds. Part II: Validation using satellite data. *J. Atmos. Sci.,* **53,** 2304–2316.

Beheng, K. D., 1994: A parameterization of warm cloud microphysical conversion processes. *Atmos. Res.,* **33,** 193–206.

Bigg, E. K., 1953: The supercooling of water. *Proc. Phys. Soc. London,* **66B,** 688–694.

Cooper, W. A., 1986: Ice initiation in natural clouds. *Precipitation Enhancement—A Scientific Challenge, Meteor. Mongr.,* No. 43, Amer. Meteor. Soc., 29–32.

Del Genio, A. D., M.-S. Yao, W. Kovari, and K. K.-W. Lo, 1996: A prognostic cloud water parameterization for climate models. *J. Climate,* **9,** 270–304.

Ferrier, B., 1994: A double-moment multiple-phase four-class bulk ice scheme. Part I: Description. *J. Atmos. Sci.,* **51,** 249–280.

Field, P. R., A. J. Heymsfield, and A. Bansemer, 2006: A test of self-collection kernels using aircraft data. *J. Atmos. Sci.,* **63,** 651–666.

Fowler, L. D., D. A. Randall, and S. A. Rutledge, 1996: Liquid and ice cloud microphysics in the CSU General Circulation Model. Part I: Model description and simulated microphysical processes. *J. Climate,* **9,** 489–529.

Gettelman, A., H. Morrison, and S. J. Ghan, 2008: A new two-moment bulk stratiform cloud microphysics scheme in the Community Atmosphere Model, version 3 (CAM3). Part II: Single-column and global results. *J. Climate,* **21,** 3660–3679.

Ghan, S. J., and R. C. Easter, 1992: Computationally efficient approximations to stratiform cloud microphysics parameterization. *Mon. Wea. Rev.,* **120,** 1572–1582.

——, L. R. Leung, and R. C. Easter, 1997: Prediction of cloud droplet number in a general circulation model. *J. Geophys. Res.,* **102,** 21 777–21 794.

Hallett, J., and S. C. Mossop, 1974: Production of secondary ice particles during the riming process. *Nature,* **249,** 26–28.

Heymsfield, A. J., A. Bansemer, and C. H. Twohy, 2007: Refinements to ice particle mass dimensional and terminal velocity relationships for ice clouds. Part I: Temperature dependence. *J. Atmos. Sci.,* **64,** 1047–1067.

Ikawa, M., and K. Saito, 1990: Description of the nonhydrostatic model developed at the Forecast Research Department of the MRI. Meteorological Institute MRI Tech. Rep., 28, 238 pp. [Available from Meteorological Research Institute, Tsukuba, Ibaraki 305-0052, Japan.]

Kärcher, B., and U. Lohmann, 2002: A parameterization of cirrus cloud formation: Homogeneous freezing including effects of aerosol size. *J. Geophys. Res.,* **107,** 4698, doi:10.1029/2001JD001429.

——, and ——, 2003: A parameterization of cirrus cloud formation: Heterogeneous freezing. *J. Geophys. Res.,* **108,** 4402, doi:10.1029/2002JD003220.

Khairoutdinov, M. F., and Y. Kogan, 2000: A new cloud physics parameterization in a large-eddy simulation model of marine stratocumulus. *Mon. Wea. Rev.,* **128,** 229–243.

Khvorostyanov, V. I., and J. A. Curry, 2005: The theory of ice nucleation by heterogeneous freezing of deliquescent CCN. Part I: Critical radius, energy, and nucleation rate. *J. Atmos. Sci.,* **61,** 2676–2689.

Larson, V. E., R. Wood, P. R. Field, J. Golaz, T. H. VonderHaar, and W. R. Cotton, 2001: Systematic biases in the microphysics and thermodynamics of numerical models that ignore subgrid-scale variability. *J. Atmos. Sci.,* **58,** 1117–1128.

Lin, Y.-L., R. D. Farley, and H. D. Orville, 1983: Bulk parameterization of the snow field in a cloud model. *J. Appl. Meteor.,* **22,** 1065–1089.

Liu, J. Y., and H. D. Orville, 1969: Numerical modeling of precipitation and cloud shadow effects on mountain-induced cumuli. *J. Atmos. Sci.,* **26,** 1283–1298.

Liu, X., J. E. Penner, S. J. Ghan, and M. Wang, 2007: Inclusion of ice microphysics in the NCAR Community Atmosphere Model version 3 (CAM3). *J. Climate,* **20,** 4526–4547.

Locatelli, J. D., and P. V. Hobbs, 1974: Fall speeds and masses of solid precipitation particles. *J. Geophys. Res.,* **79,** 2185–2197.

Lohmann, U., 2002: Possible effects on ice clouds via contact nucleation. *J. Atmos. Sci.,* **59,** 647–656.

——, and E. Roeckner, 1996: Design and performance of a new cloud microphysics scheme developed for the ECHAM general circulation model. *Climate Dyn.,* **12,** 557–572.

——, J. Feichter, C. C. Chuang, and J. E. Penner, 1999: Prediction of the number of cloud droplets in the ECHAM GCM. *J. Geophys. Res.,* **104,** 9169–9198.

Martin, G. M., D. W. Johnson, and A. Spice, 1994: The measurement and parameterization of effective radius of droplets in warm stratocumulus clouds. *J. Atmos. Sci.,* **51,** 1823–1842.

Meyers, M. P., R. L. Walko, J. Y. Harrington, and W. R. Cotton, 1997: New RAMS cloud microphysics parameterization. Part II: The two-moment scheme. *Atmos. Res.,* **45,** 3–39.

Milbrandt, J. A., and M. K. Yau, 2005: A multimoment bulk microphysics parameterization. Part I: Analysis of the role of the spectral shape parameter. *J. Atmos. Sci.,* **62,** 3051–3064.

Ming, Y., V. Ramaswamy, L. J. Donner, V. T. Phillips, S. A. Klein, P. A. Ginoux, and L. W. Horowitz, 2007: Modeling the interactions between aerosols and liquid water clouds with a self-consistent cloud scheme in a general circulation model. *J. Atmos. Sci.,* **64,** 1189–1209.

Morrison, H., and J. O. Pinto, 2005: Mesoscale modeling of springtime arctic mixed-phase stratiform clouds using a new two-moment bulk microphysics scheme. *J. Atmos. Sci.,* **62,** 3683–3704.

——, and W. W. Grabowski, 2007: Comparison of bulk and bin warm-rain microphysics models using a kinematic framework. *J. Atmos. Sci.,* **64,** 2839–2861.

——, J. A. Curry, and V. I. Khvorostyanov, 2005: A new double-moment microphysics scheme for application in cloud and climate models. Part I: Description. *J. Atmos. Sci.,* **62,** 1665–1677.

Phillips, V. T., L. J. Donner, and S. T. Garner, 2007: Nucleation processes in deep convection simulated by a cloud-resolving model with double-moment microphysics. *J. Atmos. Sci.,* **64,** 738–761.

Pincus, R., and S. A. Klein, 2000: Unresolved spatial variability and microphysical process rates in large-scale models. *J. Geophys. Res.,* **105,** 27 059–27 065.

——, S. A. McFarlane, and S. A. Klein, 1999: Albedo bias and the horizontal variability of clouds in subtropical marine boundary layers: Observations from ships and satellite. *J. Geophys. Res.,* **104,** 6183–6191.

Pruppacher, H. R., and J. D. Klett, 1997: *Microphysics of Clouds and Precipitation*. Kluwer Academic, 954 pp.

Rasch, P. J., and J. E. Kristjansson, 1998: A comparison of the CCM3 model climate using diagnosed and predicted condensate parameterizations. *J. Climate,* **11,** 1587–1614.

Reisner, J., R. M. Rasmussen, and R. T. Bruintjes, 1998: Explicit forecasting of supercooled liquid water in winter storms using the MM5 forecast model. *Quart. J. Roy. Meteor. Soc.,* **124,** 1071–1107.

Rotstayn, L. D., 1997: A physically based scheme for the treatment of stratiform cloudfs and precipitation in large-scale models. I: Description and evaluation of the microphysical processes. *Quart. J. Roy. Meteor. Soc.,* **123,** 1227–1282.

——, B. F. Ryan, and J. J. Katzfey, 2000: A scheme for calculation

of the liquid fraction in mixed-phase stratiform clouds in large-scale models. *Mon. Wea. Rev.,* **128,** 1070–1088.

Seifert, A., and K. D. Beheng, 2001: A double-moment parameterization for simulating autoconversion, accretion, and self-collection. *Atmos. Res.,* **59–60,** 265–281.

Stephens, G. L., 2005: Cloud feedbacks in the climate system: A critical review. *J. Climate,* **18,** 1149–1152.

——, and Coauthors, 2002: The CloudSat mission and the A-train: A new dimension of space-based observations of clouds and precipitation. *Bull. Amer. Meteor. Soc.,* **83,** 1771–1790.

Thompson, G., R. M. Rasmussen, and K. Manning, 2004: Explicit forecasts of winter precipitation using an improved bulk microphysics scheme. Part I: Description and sensitivity analysis. *Mon. Wea. Rev.,* **132,** 519–542.

——, P. R. Field, R. M. Rasmussen, and W. D. Hall, 2008: Explicit forecasts of winter precipitation using an improved bulk microphysics scheme. Part II: Implementation of a new snow parameterization. *Mon. Wea. Rev.,* in press.

Tompkins, A. M., 2002: A prognostic parameterization for the subgrid-scale variability of water vapor and clouds in large-scale models and its use to diagnose cloud cover. *J. Atmos. Sci.,* **59,** 1917–1942.

Twomey, S., 1977: The influence of pollution on the shortwave albedo of clouds. *J. Atmos. Sci.,* **34,** 1149–1152.

Zhang, M., W. Lin, C. S. Bretherton, J. J. Hack, and P. J. Rasch, 2003: A modified formulation of fractional stratiform condensation rate in the NCAR Community Atmosphere Model (CAM2). *J. Geophys. Res.,* **108,** 4035, doi:10.1029/2002JD002523.